Kawai et al. *NPG Asia Materials* (2022) 14:32
https://doi.org/10.1038/s41427-021-00348-2

NPG Asia Materials

ARTICLE Open Access

Preparation of dual-cross network polymers by the knitting method and evaluation of their mechanical properties

Yusaku Kawai[1], Junsu Park[1], Yoshiki Ishii[2], Osamu Urakawa[1], Shunsuke Murayama[3], Ryohei Ikura[1], Motofumi Osaki[1,4], Yuka Ikemoto[5], Hiroyasu Yamaguchi[1,4,6], Akira Harada[7], Tadashi Inoue[1,4], Hitoshi Washizu[2], Go Matsuba[3] and Yoshinori Takashima[1,4,6,8]

Abstract

Bulk copolymerization of alkyl acrylates and cyclodextrin (CD) host monomers produced a single movable cross-network (SC). The CD units acted as movable crosslinking points in the obtained SC elastomer. Introducing movable crosslinks into a poly(ethyl acrylate/butyl acrylate) copolymer resulted in good toughness (G_f) and stress dispersion. Here, to improve the Young's modulus (E) and G_f of movable cross-network elastomers, the bulk copolymerization of liquid alkyl acrylate monomer swelling in SC gave another type of movable cross-network elastomer with penetrating polymers (SCPs). Moreover, the bulk copolymerization of alkyl acrylate and the CD monomer in the presence of SC resulted in dual cross-network (DC) elastomers. The G_f of the DC elastomer with a suitable weight % (wt%) of the secondary movable cross-network polymer was higher than those of the SCP or SC elastomers. The combination of suitable hydrophobicity and glass transition of the secondary network was important for improving G_f. Small-angle X-ray scattering (SAXS) indicated that the DC elastomers exhibited heterogeneity at the nanoscale. The DC elastomers showed a significantly broader relaxation time distribution than the SC and SCP elastomers. Thus, the nanoscale heterogeneity and broader relaxation time distribution were important to increase G_f. This method to fabricate SCP and DC elastomers with penetrating polymers would be applicable to improve the G_f of conventional polymeric materials.

Introduction

In recent years, various polymer networks have been reported to create new functional materials[1–7]. These unique polymer networks have attracted much attention for their innovative mechanical properties and functions, which are difficult to achieve by conventional synthetic methods, such as copolymerization and polymer mixing (polymer alloys and blends)[8,9], interpenetrating polymers (IPNs)[10] and double-network polymers[11,12]. Recently, polymeric materials with reversible or movable crosslinkers have been employed to achieve new functions, such as effective stress relaxation, high toughness (G_f), and self-healing properties[13–24]. When preparing a polymeric material with movable crosslinkers, cyclic molecules are required to penetrate the polymer chain[25–30]. Preorganized polyrotaxane is an effective polymer component to prepare movable crosslinked materials[31–33]. The introduction of reversible or movable crosslinkers is an effective method to improve the mechanical properties beyond those obtained by covalently crosslinked polymeric materials. Generally, fabrication techniques, such as mixing polymers or fillers with different physical properties, have been chosen to prepare a highly elastic

Correspondence: Akira Harada (harada@chem.sci.osaka-u.ac.jp) or Hitoshi Washizu (h@washizu.org) or Go Matsuba (gmatsuba@yz.yamagata-u.ac.jp) or Yoshinori Takashima (takasima@chem.sci.osaka-u.ac.jp)
[1]Department of Macromolecular Science, Graduate School of Science, Osaka University, 1-1 Machikaneyama, Toyonaka, Osaka, Japan
[2]Graduate School of Information Science, University of Hyogo, 7-1-28 Minatojima-minamimachi, Chuo-ku, Kobe, Hyogo, Japan
Full list of author information is available at the end of the article

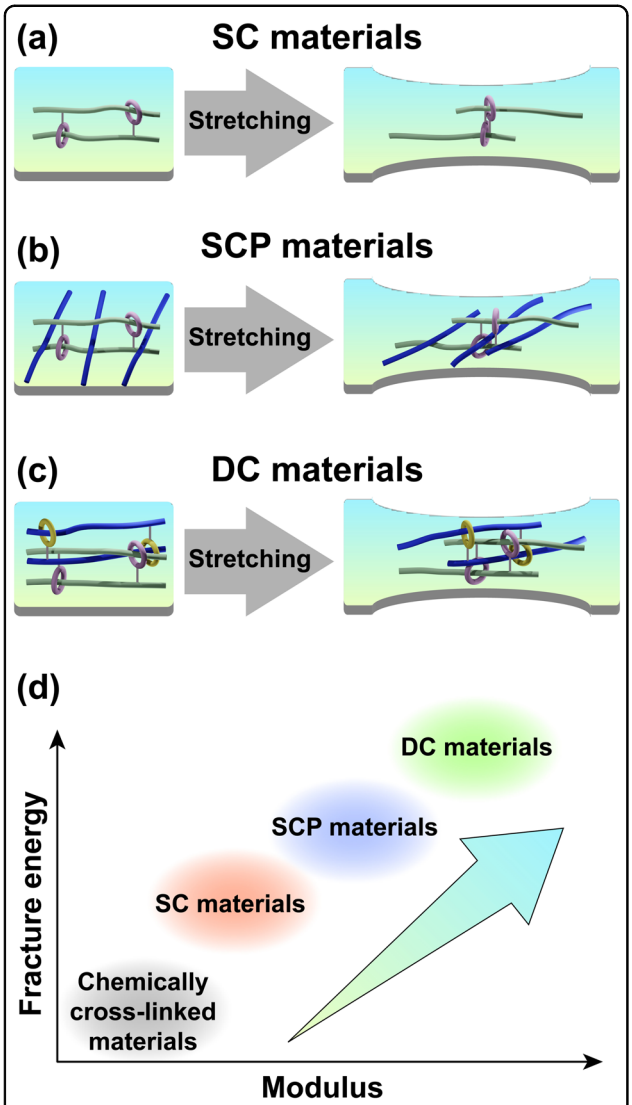

Fig. 1 Schematics of the polymeric materials with different preparation structures. a Single movable cross-network elastomers (SC elastomers), **b** single movable cross-network elastomers with penetrating polymer chains (SCP elastomers), and **c** dual movable cross-network elastomers (DC elastomers). **d** Proposed mechanical property map of the toughness and modulus of these elastomers.

material with great G_f. To produce a material with both a high Young's modulus (E) and a high G_f, which are usually involved in a trade-off relationship, we proposed new molecular and material designs.

Previously, we prepared movable crosslinking elastomers using acrylate-based polymers or acrylamide-based polymers as the polymer main chain (Fig. 1a)[34,35], here called single movable cross-network (SC) elastomers. The G_f of these SC elastomers was higher than those of chemically crosslinked elastomers and elastomers without any crosslinking. Inoue and his coworker revealed the viscoelastic behaviors and relaxation mode of the movable crosslinking of SC elastomers[36,37]. Adjusting the content (mol%) of the CD unit (the crosslinking density) or varying the main chain polymer with different glass transition temperatures (T_g values) is useful to control the elastic modulus of SC elastomers. However, improving the G_f of SC elastomers with a much higher E is challenging.

Here, we focused on the network structure of SC elastomers, which consists of two kinds of polymer networks with movable units. We propose that the first network structure has a hole into which another polymer chain penetrates. Knitting the mesh holes of the SC elastomers with another polymer chain should produce an SC network with penetrating polymer elastomers (SCPs) (Fig. 1b). The knitted polymer chains in the SCP elastomer should slide into the mesh hole to increase G_f while maintaining a high E. Furthermore, we propose a dual movable cross-network elastomer (DC), in which another SC network is knitted into the mesh hole (Fig. 1c). This DC elastomer is expected to have higher E and G_f values. To prepare SCP and DC elastomers with a high G_f, two different types of monomers were employed: a hydrophobic acrylate as the soft segment and a hydrophilic acrylamide derivative as the hard segment. Thus, the "molecular knitting method" is our strategy for tough polymers. Here, it is important to note that polymers with different polarities are generally hard to mix even if they are mixed in the molten state or polymerized as a homogeneous monomer solution. In the case of crosslinked networks, macroscopic phase separation is prevented by the network structure, but is expected to have large nanoscale concentration fluctuations. In the present case, the crosslinking point is movable, and we anticipate similar suppression of the microscopic phase separation and larger concentration fluctuations due to fewer confinement effects of the movable crosslinks. Such a large concentration fluctuation results in a broader glass transition and therefore the rubber/glass composite, as in the case of high impact polystyrene, in which rubber particles are dispersed in the glassy polystyrene matrix[38,39]. Thus, molecular knitting is our fundamental idea, but we further anticipate a toughening effect through a preferable nanoscale structure in the knitted networks. Here, we fabricated and reported SC, SCP, and DC elastomers to evaluate their mechanical properties (Fig. 1d). The DC elastomers showed significantly improved values of E and G_f.

Results and discussion

Preparation of the DC, SCP and SC elastomers

Figure 2 shows the chemical structures of the dual movable cross-network elastomers (DC(w) elastomers), the single movable cross-network elastomers with penetrating polymers (SCP(w) elastomers), and the single

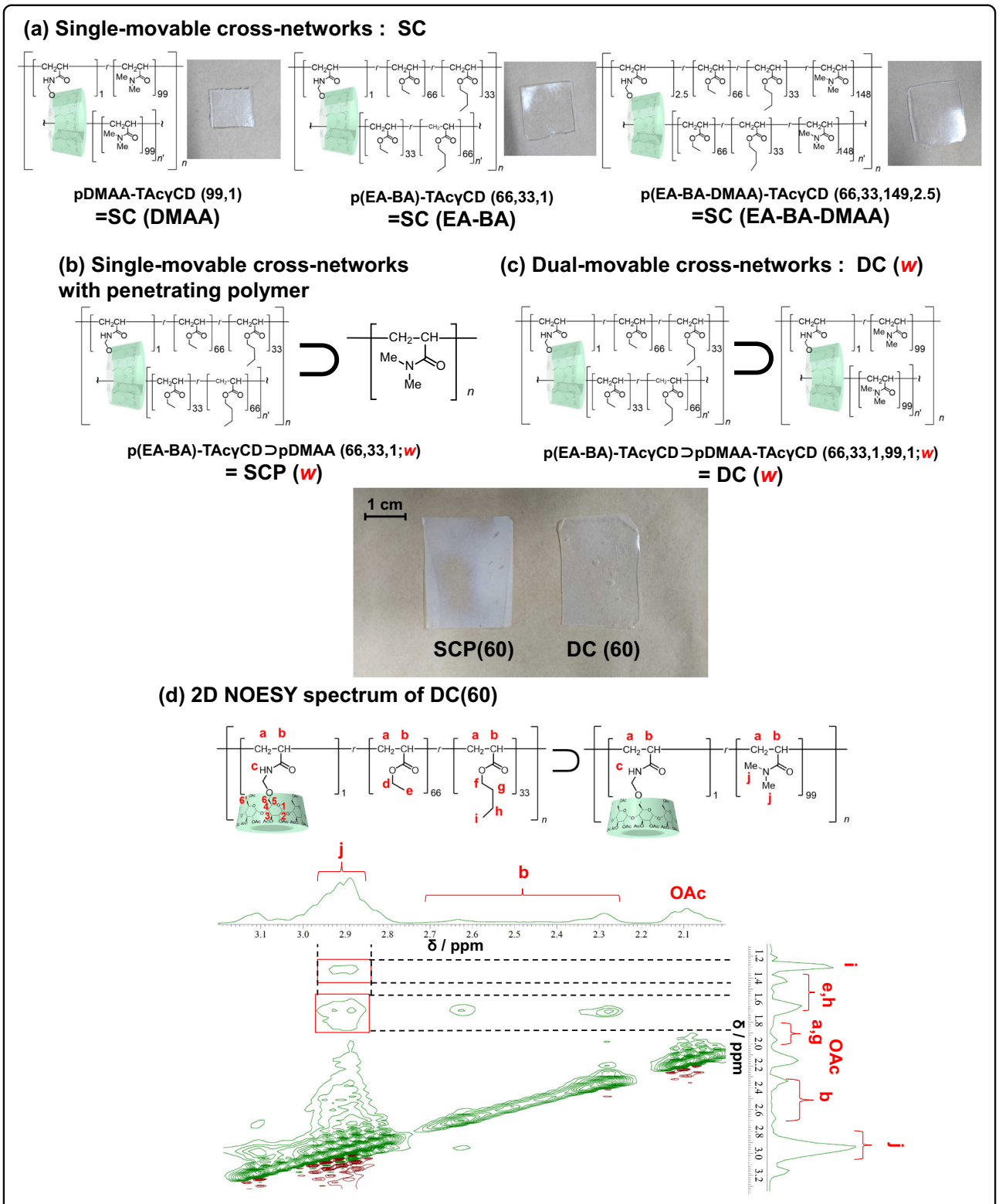

Fig. 2 Preparation of the dual movable cross-network (DC) elastomers, single movable cross-network with penetrating polymers (SCP) elastomers, and single movable cross-network (SC) elastomers. Chemical structures of **a** single movable cross-network (SC) elastomers, **b** SC with penetrating polymers (SCP(*w*)), and **c** dual movable cross-network DC(*w*). **d** The 600 MHz 2D ^{1}H-^{1}H NOESY NMR spectrum of DC(60) in $CDCl_3$.

movable cross-network elastomers (SC elastomers). The SC elastomers were prepared according to a previous report[34]. The SC elastomers were given different names, such as SC(EA-BA) (Scheme S1, Table S1, Fig. S1), SC (EA-BA-DMAA) (Scheme S2, Fig. S2), and SC(DMAA) (Scheme S3, Fig. S3), based on their main chain monomers (*N*,*N*-dimethylacrylamide (DMAA), ethyl acrylate (EA), and butyl acrylate (BA)) (Fig. 2a).

The DC(*w*) and SCP(*w*) elastomers have two individual polymer networks. The *w* values are the weight% contents of the secondary network. The SCP(*w*) elastomer was prepared by photopolymerization of DMAA with 1-hydroxy-cyclohexylphenyl-ketone (IGM Resins B.V., Omnirad 184), where the SC(EA-BA) elastomers were swollen in the monomer solution (Fig. 2b, Scheme S4, Fig. S4, and Table S2). When bulk free-radical copolymerization was carried out by UV irradiation with a high-pressure Hg lamp ($\lambda = 253$ and 365 nm), a transparent elastomer formed within 30 min. After polymerization, the elastomer was dried at 80 °C in vacuo to remove the residual DMAA. The other elastomers, DC(*w*), were prepared in the same manner (Fig. 2c, Scheme S5, Fig. S5, Tables S3 and S4). The DC(*w*), SCP(*w*) and SC elastomers were characterized by ^{1}H NMR (Figs. S1−S5) and FT-IR spectroscopy (Fig. S6). DC(60) was more transparent than SCP(60) (Fig. 2).

To spectroscopically elucidate the knitting structure between p(EA-BA)-TAcγCDAAmMe (the primary network) and pDMAA-TAcγCDAAmMe (the secondary network), 2D ^{1}H-^{1}H nuclear Overhauser effect spectroscopy (NOESY) NMR was performed to observe correlation signals in DC(60) (p(EA-BA)-TAcγCDAAmMe ⊃ pDMAA-TAcγCDAAmMe) swollen in $CDCl_3$ (the operator ⊃ indicates the interpenetrating structure). The spectra of SCP(60) (p(EA-BA)-TAcγCDAAmMe ⊃ pDMAA) (Fig. S7) and SC(EA-BA-DMAA) (p(EA-BA-DMAA)-TAcγCDAAmMe) (Fig. S8) did not exhibit NOE correlations between the protons of the main chain polymers, indicating that the SC and SCP elastomers do not form a spatially dense structure between the main chain polymers. On the other hand, the spectrum of DC(60) swollen in $CDCl_3$ exhibited NOE correlations between the protons in the p(EA-BA) polymer and the protons on the pDMAA main chain (Fig. 2d), suggesting a significantly close distance between the primary and secondary networks. DC(60) should form the knitting network structure between p(EA-BA)-TAcγCDAAmMe (the primary network) and pDMAA-TAcγCDAAmMe (the secondary network).

Simulation of the mixed state of 4 kinds of monomers

In the current polymerization method, EA, BA, DMAA, and TAcγCDAAmMe were mixed simultaneously without any solvent. EA and BA are hydrophobic liquid monomers, and DMAA and TAcγCDAAmMe are relatively hydrophilic monomers. Then, an all-atom molecular dynamics (MD) simulation was carried out to investigate the structural properties of the mixed solutions, including the four kinds of monomers. The mesoscale structures of the monomer mixtures, radial distribution functions and their potentials of mean force were evaluated by MD simulations of the pairs of TAcγCDAAmMe and the other monomer species. Our simulations indicated that the monomers EA, BA and DMAA were relatively dispersed in the monomer solutions, and then, the TAcγCDAAmMe monomer aggregated slightly regardless of the composition in the MD system (Fig. 3a, b, c).

On the basis of the materials perspective of network polymers, the reason for selecting the acrylamide-based monomer DMAA for the acrylate-based monomers EA and BA was to consider the penetration efficiency of TAcγCDAAmMe into the cavity in addition to the T_g of poly(DMAA). Spectroscopic analyses in our previous reports showed that poly(EA) and poly(DMAA) penetrated into the cavity of TAcγCDAAmMe, and we confirmed the improvement in G_f[34,35]. We expected DMAA to penetrate the cavity of γCD more easily than EA. This scenario was revisited through MD simulations. First, either acrylate or DMAA monomers were mixed with TAcγCDAAmMe to evaluate their penetration into the TAcγCDAAmMe cavity. From MD simulations of 14 compositions, the EA and DMAA monomers were stabilized in the cavity of TAcγCDAAmMe (Fig. 3d, Table S5). BA also entered the cavity, but the penetration probability was lower than that when EA and DMAA were used. Next, TAcγCDAAmMe was mixed with a certain mixing ratio of EA/BA/DMAA in the MD simulation. The mixing ratio of [EA]/[BA]/[DMAA] = 200/100/500 effectively formed complexes with strong binding free energies of the monomers (Fig. 3e, Fig. S9). Based on the above results, DMAA was selected as an acrylamide-based monomer for EA and BA, and the mixing ratio of EA/BA/DMAA was referenced to prepare the DC, SCP, and SC elastomers.

Mechanical properties of the DC, SCP, SC elastomers

Tensile tests determined the mechanical properties of the DC(*w*), SCP(*w*), and SC elastomers. Figure 4a shows the stress−strain curves of DC(60), SCP(60), and SC(EA-BA-DMAA). The fracture stresses (σ) of DC(60) and SCP(60) are not very different, but the fracture strain (λ) of DC(60) is approximately twice that of SCP(60). Figure 4b shows the relationship between G_f of the SCP(*w*) elastomers and SC(EA-BA) and *w* of the secondary network of pDMAA. G_f was evaluated as the integral of the strain −stress curve from the tensile tests. G_f of the SCP(*w*) elastomers increased with *w* and reached a maximum at

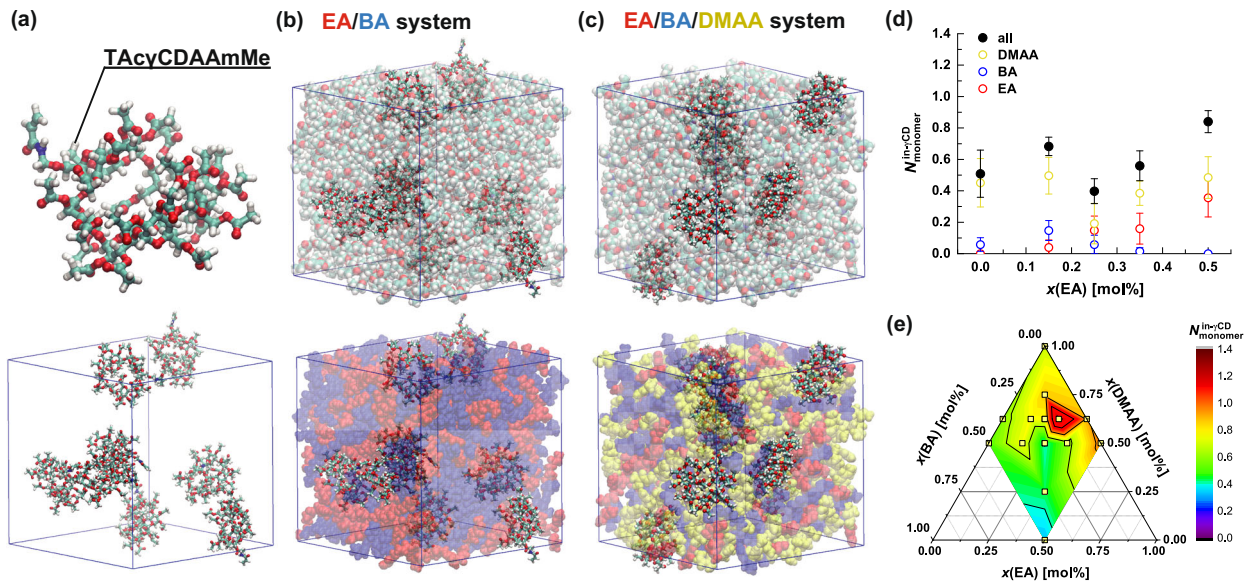

Fig. 3 MD simulations with a mixture of four kinds of monomers (EA, BA, DMAA, and TAcγCDAAmMe). Investigation of a suitable monomer ratio to penetrate into the cavity of TAcγCDAAmMe. **a** Snapshots of an isolated monomer of TAcγCDAAmMe and the system image in the monomer solution. **b**, **c** Snapshots of MD simulations in monomer solutions of (**b**) [EA]/[BA]/[TAcγCDAAmMe] = 400/400/8 and **c** [EA]/[BA]/[DMAA]/[TAcγCDAAmMe] = 200/200/400/8 (right). **d** The calculated number of monomers included in the TAcγCDAAmMe cavity with various composites ([EA]/[BA]/[DMAA] = 200*x*/200/400(1-*x*)). **e** The three-component diagram estimated from the calculated number of monomers included in the TAcγCDAAmMe cavity.

$w = 60$ wt%. Figure 4c shows the relationship between G_f and E of the SCP(w) elastomers and the control polymer, SC(EA-BA-DMAA). Hard materials with a high E are generally brittle with a low G_f. However, the G_f values of the SCP(w) elastomers increased with increasing w of the penetrating pDMAA and reached its maximum at 60 wt%. The G_f of SCP(60) was significantly higher than those of SC(EA-BA) as the primary network and native pDMAA. These results indicate that a suitable wt% of the penetrating pDMAA as the secondary network plays a role in improving both G_f and E.

Figure 4d shows the stress−strain curves of the DC(w) elastomers, which depend on the wt% of the secondary movable polymer network. DC(60) exhibited a higher G_f than SC(EA-BA-DMAA) and SCP(60); however, G_f depends on w in a similar manner to the SCP(w) elastomers. We also investigated a suitable molar ratio of EA:BA in the SC(EA-BA) primary network of DC(60) (Fig. S10). The G_f of DC(60) with 66 mol% EA in SC(EA-BA) was higher than that in SC(EA-BA). Figure 4e shows that the highest G_f values of the DC(w) elastomers were found at approximately 40–60 wt% of the secondary movable crosslinking network. We also studied the effect of the stiffness of the primary network on the mechanical properties. We prepared DC(DMAA⊃EA)(w), which has SC(DMAA) as the primary polymer and SC(EA) as the secondary polymer. Fig. S11 shows the mechanical properties of DC(DMAA⊃EA)(w). The G_f of DC (DMAA⊃EA)(w) was lower than that of SC(EA), which does not contain a primary polymer. This result implies that the soft primary network (SC(EA-BA)) is important to prepare tough polymeric materials.

Figure 4f summarizes the relationship between G_f and E for the movable crosslinked elastomers and G_f of the SC elastomers (SC(EA-BA), SC(EA-BA-DMAA), and SC (DMAA)), which were almost the all same and at a similarly low level. The E of the SC elastomers increased with T_g, meaning that E can be controlled by changing the polymer main chain structure, but further improving G_f at the same time is difficult. On the other hand, adjusting the wt% of the secondary network in the DC(w) and SCP(w) elastomers enables the control of G_f. If the secondary network of DC(60) was replaced with a chemically crosslinked network, here, called DCC(60) (Scheme S6), the G_f of DCC(60) was significantly lower than that of DC (60) (Fig. S12). These results indicate that the molecular knitting method provides simultaneous improvements in both G_f and E.

We next investigated the effect of the movable crosslinks with cyclic tensile tests of SCP(60) and DC(60) (Fig. 4g, h). Test pieces were continuously stretched and recovered without rest intervals. The maximum strains of SCP(60) were set to 10%, 50%, and 100% with a deformation rate of 1.0 mm/s (Fig. 4g). In the DC(60) test, the strains were set to 10%, 50%, 100%, 150%, 200% and 250% (Fig. 4h). Figure 4i shows the plots of the hysteresis losses

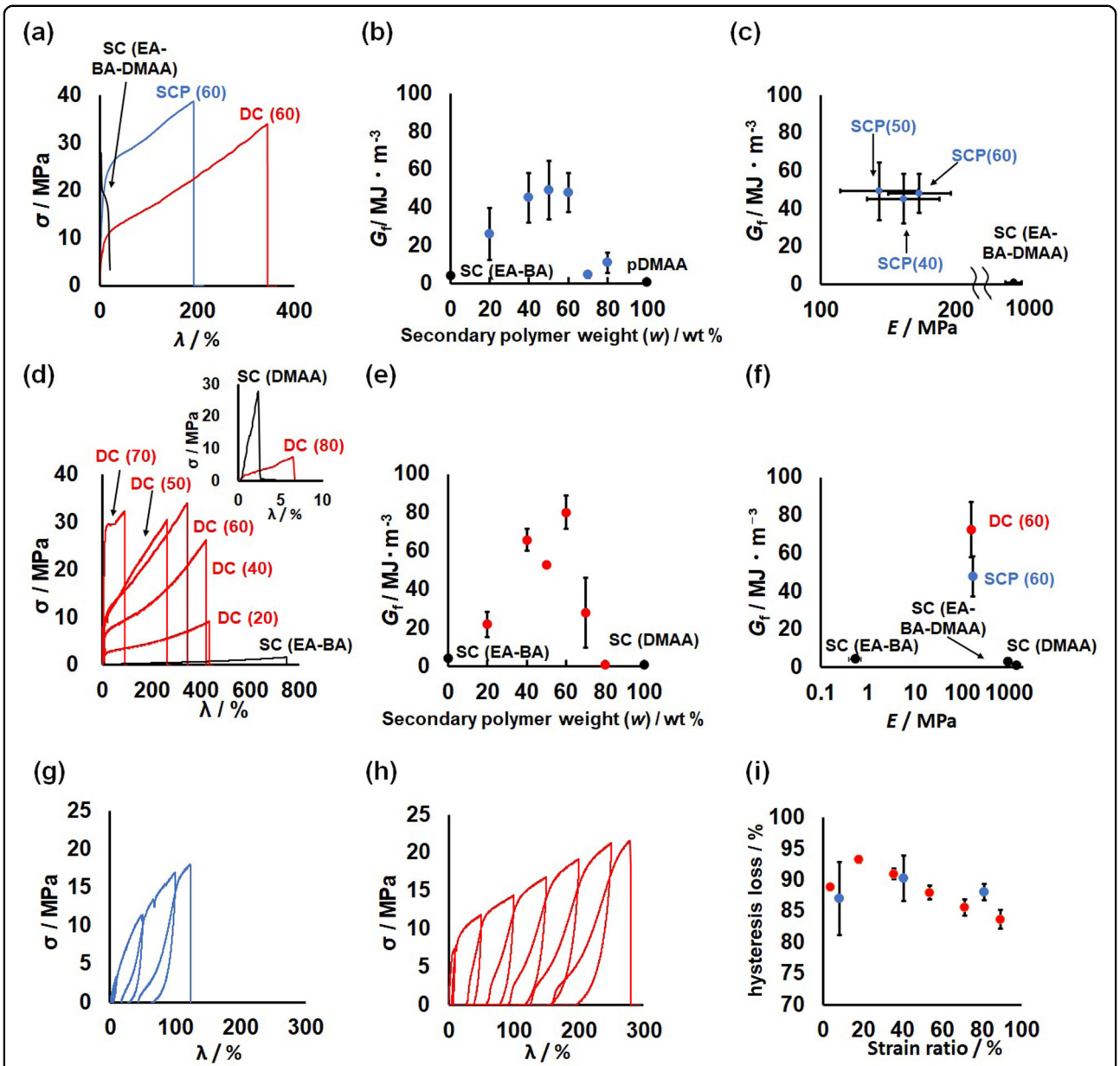

Fig. 4 Mechanical properties of the dual- and single-movable cross-network elastomers. a Stress–strain curves of DC(60) (red line), SCP(60) (blue line), and SC(EA-BA-DMAA) (black lines). **b** Plots of toughness (G_f) versus weight fraction of the secondary network (w) of SCP(w) (blue circles), SC(EA-BA) and pDMAA. **c** Plots of G_f versus Young's modulus (E) of SCP(w) (blue circles) and SC(EA-BA-DMAA) (black circles). **d** Stress–strain curves of DC(w) (red lines) and SC(DMAA) and SC(EA-BA) (black lines). **e** Plots of G_f versus the weight fraction of the secondary network (w) of DC(w) (red circles), SC(EA-BA) and SC(DMAA) (black circles). **f** Plots of G_f versus E of DC(60) (red circle), SCP(60) (blue circle), SC(EA-BA-DMAA), SC(DMAA) and SC (EA-BA) (black circles). **g**, **h** Stress (σ)-strain (λ) curves of SCP(60) (blue lines) and DC(60) (red lines) obtained from the cyclic tensile tests. **i** Plots of hysteresis loss versus λ for SCP(60) (blue circles) and DC(60) (red circles). The strain ratios were normalized by the elongation ratio at break.

of SCP(60) and DC(60) depending on the cycle, which were calculated using the following equation:

$$\text{Hysteresis loss}\,(\%) = (W_{\text{out}} - W_{\text{in}})/W_{\text{in}} \times 100(\%)$$

W_{in}: work added to the test piece during stretching

W_{out}: work recovered from the test piece through shrinking.

W_{in} and W_{out} were determined from the stress-strain curve from the cyclic tensile tests. SCP(60) and DC(60) both exhibited high hysteresis loss, indicating that excess movable crosslinking prevents recovery of the initial sample form.

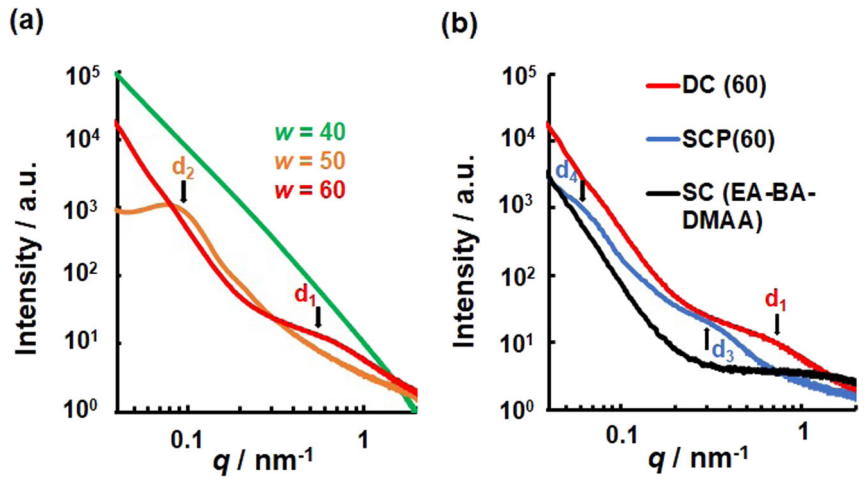

Fig. 5 Structural information of the DC, SCP, and SC elastomers by SAXS measurements. a SAXS profiles of DC(*w*) (*w* = 40, 50 and 60). **b** SAXS profiles of DC(60) (red line), SCP(60) (blue line), and SC(EA-BA-DMAA) (black line).

SCP(60) showed almost constant hysteresis regardless of the strain ratio, while DC(60) showed a slight decrease in hysteresis as the strain ratio increased, which was normalized by the elongation ratio at break (Fig. 4i). This result indicates that the structure of DC(60) is more likely to recover its original structure after stretching.

Structural information of the DC, SCP and SC elastomers

We investigated the internal structures of the topologically crosslinked elastomers by small-angle X-ray scattering (SAXS) measurements to elucidate the nanoscale structure. Figure 5a shows the SAXS profiles of DC(60), DC(50), and DC(40), in which the G_f values were higher than those of the other DCs(*w*). DC(60) and DC(50) displayed peaks d_1 and d_2 at 0.60 and 0.10 nm^{-1} of the scattering vector (*q*), corresponding to domain spacing sizes of 8.3 nm and 50 nm, respectively. DC(40) continued to increase over the whole detected range. DC(60) was confirmed to have heterogeneity at the nanoscale, which implied dispersion of the nanodomains, Fig. 5b shows that SCP(60) had two peaks; the d_3 and d_4 values of 0.30 and 0.060 nm^{-1} corresponded to domain spacing sizes of 21 and 94 nm, respectively. The domain spacing sizes of DC(60) were smaller than those of SCP(60). Unlike DC(60) and SCP(60), no significant peak was observed for SC(EA-BA-DMAA), suggesting that the copolymerization of EA, BA, and DMAA resulted in a homogeneous internal structure without significant phase separation. On the other hand, d_1~d_4 of DC(60) and SCP (60) refer to domains formed by phase separation of the primary and secondary networks.

The thermal properties of DC(60), SCP(60) and SC(EA-BA-DMAA) were evaluated by DSC measurements. While SC(EA-BA-DMAA) showed a clear $T_g = 36.5$ °C on the first scan, DC(60) and SCP(60) had moderate endothermic transitions through three thermal transitions at temperatures of approximately −16 °C, 36 °C, and 90 °C (Fig. S13). On the first scan, SC(EA-BA) as the primary network was confirmed to be $T_g = -19.4$ °C, and the T_g of the secondary network pDMAA was 77.8 °C (Fig. S14). These results suggest that the two thermal transitions of DC(60) and SCP(60) were thermal transitions of the primary network and the secondary network. However, DC (60) and SCP(60) showed two clear T_g values derived from the primary network and the secondary network on the second scan (Fig. S15). SC(EA-BA) showed a $T_g = -15.2$ °C on the second scan, which was derived from the single network (Fig. S16). The primary and secondary networks mixed in DC(60) and SCP(60) were due to the knitted structures, unless they were annealed at 200 °C. The transition at approximately 36 °C observed in the first scan for DC(60) and SCP(60) disappeared after annealing. Before annealing, the primary and secondary networks mixed very well, and some phases in the as-prepared DC(60) and SCP (60) behaved as pseudo-SC(EA-BA-DMAA). According to the SAXS results, DC(60) showed smaller phase separation (~10 nm) than SCP(60). This small phase separation structure of DC(60) contributes to the high G_f.

Dependence of G_f on the distribution of relaxation modes

Figure 6 shows the composite curves of the moduli (E' and E'') of DC(60), SCP(60), and SC(EA-BA-DMAA) measured by dynamic mechanical analysis (DMA). The stretching strain for the samples was set to 0.1%, which is in the linear response regime. The storage modulus (E') and loss modulus (E'') were measured by applying sinusoidal strain at 13 different frequencies (*f*: 0.25, 0.40, 0.63, 1.0, 1.6, 2.5, 4.0, 6.3, 10, 16, 25, 40, and 63 Hz) under isothermal conditions. The same measurements were repeated at several temperatures from 5 °C to 95 °C. The composite curves of E' and E'' were constructed following

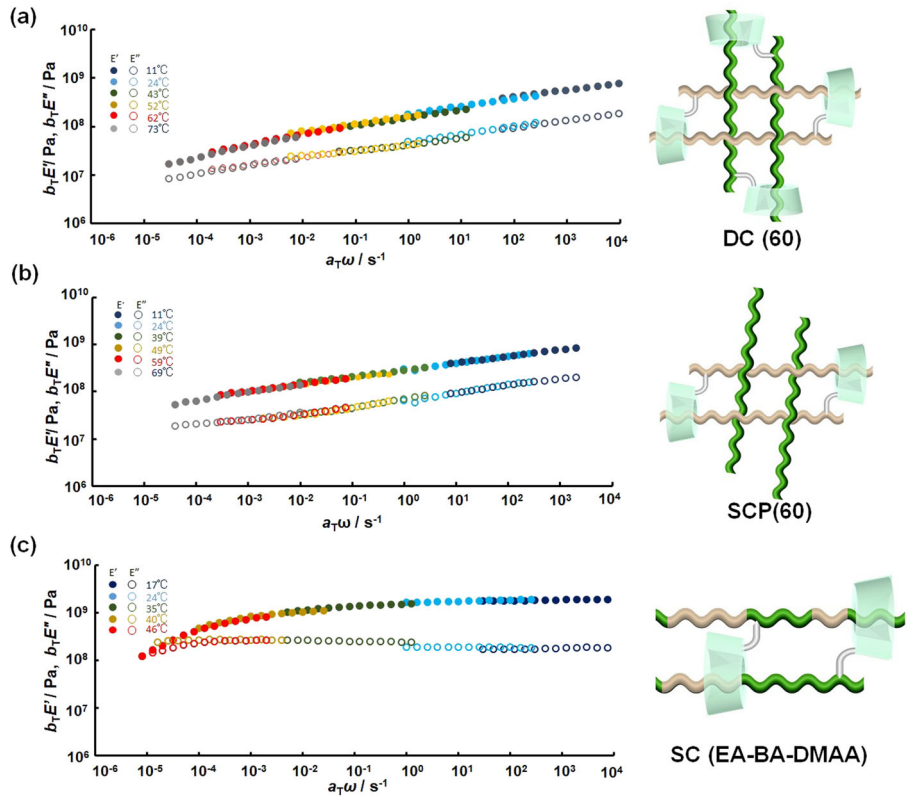

Fig. 6 Evaluation of relaxation modes of DC, SCP, and SC elastomers. Composite curves of the moduli (E' and E'') of **a** DC(60), **b** SCP(60), and **c** SC(EA-BA-DMAA).

the time (frequency)-temperature superposition principle: each modulus was a horizontally shifting modulus using the horizontal shift factor, a_T, setting 24 °C as the reference temperature, in addition to using the small vertical shift factor, $b_T \sim T/T_r$, (Figs. S17–S19). Since the time-temperature superposition principle held in this instance, we will discuss the polymer chain dynamics using the composite curves. Here, we note that $E''(\omega)$ reflects the viscoelastic relaxation time spectrum $H(\tau) \sim E''(1/\omega)$, where ω refers to the angular frequency, $\omega = 2\pi f$.

The E' values of DC(60) and SCP(60) were higher than the E'' of each material. The E' and E'' of DC(60) and SCP(60) gradually decreased with decreasing reduced frequency in the measured range. Correspondingly, the tan δ ($= E''/E'$) spectra shown in Fig. S20 are nearly independent of the frequency, suggesting a broad relaxation time distribution (Fig. 6a, b). Furthermore, the E'' of DC(60) decreased constantly while that of SCP(60) changed to a slightly flatter slope at approximately $\omega = 10^{-3}$ s^{-1}, indicating that DC(60) has longer relaxation times than SCP(60). In contrast, the E' and E'' of SC(EA-BA-DMAA) significantly decreased at a lower frequency ($\omega < 10^{-4}$ s^{-1}) (Fig. 6c), indicating a clear break (discontinuity) of the relaxation time distribution. SC (EA-BA), as the primary network, had the top of tan δ around $\tau = \omega^{-1} = 10^{-1}$ s (Fig. S21) derived from the sliding motion of the movable crosslinks[36,37]. The control sample, poly(EA) without a CD unit, did not show a marked relaxation around $\tau = 10^{-1}$ s. This means that DC(60) and SCP(60) have fast relaxation modes derived from the sliding motion of the movable crosslinks and segmental motion of the primary network. The relaxation mode at approximately $\tau = 10^3$ s was derived from a mixture of the primary network and the secondary network. Then, the decrease in E'' of DC(60) after 10^3 s can be explained by the small phase separation, as shown in the SAXS (Fig. 5b). We conducted stress relaxation tests at room temperature (Fig. S22). DC (60) and SCP(60) relaxed quickly (time > 1 s). On the other hand, SC(EA-BA-DMAA) relaxed later (time > 100 s). By DMA, DC(60) and SCP(60) showed relaxation behaviors at room temperature, while SC(EA-BA-DMAA) did not. According to the results, DC(60), SCP(60), and SC(EA-BA-DMAA) behaved similarly in the stress relaxation experiments and DMA. We note here that the glassy relaxation modes originating from segmental motions show strong plasticity. In this context, the broad relaxation time distributions would strongly result in broad energy dissipation mechanisms over a wide time frame and on special scales. This would provide better energy dissipation, particularly for

inhomogeneous deformation including cracks, where the strain rates are spatially inhomogeneous. Thus, we speculate that the broad relaxation time distributions observed for DC (60) and SCP(60) are necessary to achieve energy dissipation, which improves the G_f of DC(60) and SCP(60). Furthermore, the existence of nanoscale phase-separated interfaces, as revealed by SAXS, also improved the material's G_f, as is the case for the rubbery phase in high-impact polystyrenes.

To fabricate elastomers with the broad viscoelastic spectra shown in Fig. 6, control of the nanoscale phase-separated structure is essential. The molecular knitting method based on the movable crosslinking structure can be an effective method to achieve this material design.

Conclusion

We prepared mixed polymeric materials, dual cross-network (DC) elastomers with a knitting structure and single movable cross-network elastomers with penetrating polymers (SCP elastomers), by swelling the single movable cross-network (SC) elastomers in liquid monomers followed by photoinitiated polymerization. However, it is impossible to apply the same method to chemically crosslinked elastomers whose crosslinks are fixed. New molecular designs were achieved by the movable crosslinks in SC elastomers. DC(60) showed high toughness (G_f: 72.4 MJ • m^{-3}) and a high Young's modulus (E: 158 MPa). Figure 7a shows the plot of G_f versus E for DC(60), SCP (60), and other elastomers. The mechanical properties of DC(60) were similar to those of commercialized materials. The wide choice for the secondary network is a feature of the newly proposed material design, which maintained sufficient mechanical properties. We believe that simultaneously having high mechanical properties and flexibility in network combinations will become more important in the future. We expect that DC(60) is available for practical use. Figure 7b shows plots of $G_f \bullet E^{-1}$ versus E for SC, SCP, DC, and other elastomers. From the correlation diagram, the differences in the mechanical properties of these network elastomers can be compared more clearly. $G_f \bullet E^{-1}$ of the SC elastomers decreased monotonically with increasing E. Each SC elastomer plot falls on a straight line. On the other hand, the slope of the decrease in $G_f \bullet E^{-1}$ becomes more gradual for the SCP elastomers and even more so for the DC elastomers. The plots of the SCP and DC elastomers deviate from the linear region shown by the primary network SC elastomers, indicating that the SCP and DC elastomers have different mechanical properties. DC(60) was transparent with a phase separation structure (~10 nm) and had a long-range single mechanical relaxation mode and endothermic properties over a wide temperature range. The dynamic mechanical analysis revealed a very long single relaxation in DC(60) that showed the most improved G_f. The knitted structure of DC(60) gave a wide-ranging cooperative relaxation mode consisting of primary and secondary networks based on nanoscale heterogeneity. The achievements in this work should provide a design guide for the fabrication of new tough polymeric materials and their composites.

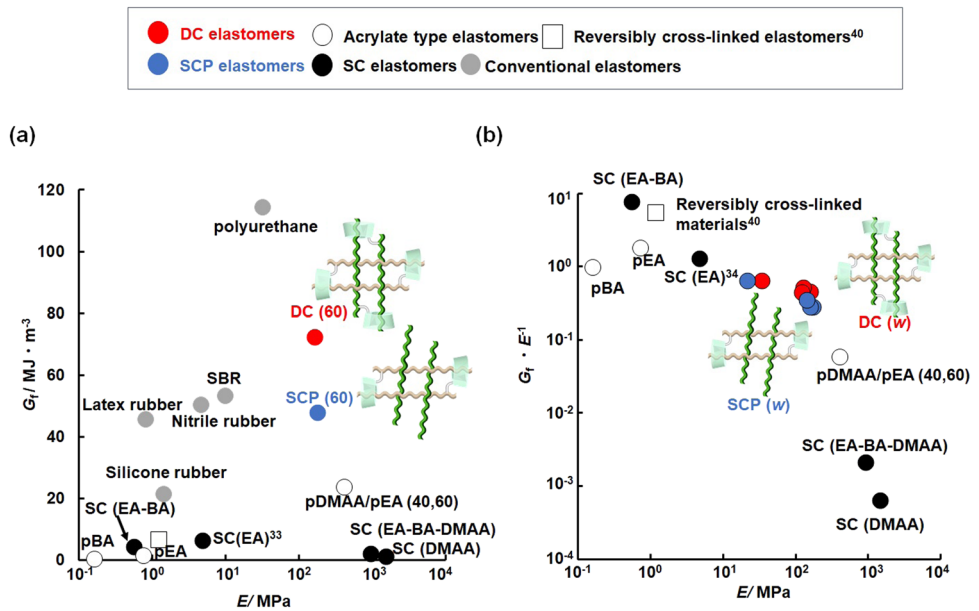

Fig. 7 Plots of G_f versus E for the various elastomers. a DC (60) (red filled circle), SCP(60) (blue filled circle), SC elastomers (black filled circle), acrylate polymer (open circle), reversibly crosslinked elastomers (open square), and conventional materials (gray filled circle). Plots of $G_f \bullet E^{-1}$ versus E for the various elastomers. **b** DC(w) (red filled circle), SCP(w) (blue filled circle), SC elastomers (black filled circle), acrylate polymer (open circle) and reversibly crosslinked elastomers (open square)[40].

Acknowledgements
This research was funded by a Grant-in-Aid for Scientific Research (B) (JP18H02035) from JSPS of Japan, Scientific Research on Innovative Area JP19H05717, JP19H05718, and JP19H05721 from MEXT of Japan, the JST-Mirai Program Grant Number JPMJMI18E3, the Ogasawara Foundation for the Promotion of Science & Engineering, the Asahi Glass Foundation, the Kao Foundation for Arts and Sciences, and the Yazaki Memorial Foundation for Science. We also want to express our gratitude to the Murata Science Foundation and ENEOS Tonen-general Research/Development Encouragement & Scholarship Foundation. The authors also appreciate the Analytical Instrument Faculty of Graduate School of Science, Osaka University, for supporting the NMR and DSC measurements. The authors would like to thank Dr. Noboru Ohta (SPring-8, JASRI) for the synchrotron radiation scattering measurements. The synchrotron radiation experiments were performed at BL40B2 (proposal no. 2021A1593) and BL43IR (proposal no. 2020A1524) of SPring-8 with the approval of the Japan Synchrotron Radiation Research Institute (JASRI). The MD calculations were performed by using the supercomputers of Osaka University (OCTOPUS), Hokkaido University (Grand Chariot), the Research Center for Computational Science at Okazaki, and Kyushu University (ITO), partially through the HPCI System Research Project (Project IDs: hp200043, hp210062, and hp210110).

Author details
[1]Department of Macromolecular Science, Graduate School of Science, Osaka University, 1-1 Machikaneyama, Toyonaka, Osaka, Japan. [2]Graduate School of Information Science, University of Hyogo, 7-1-28 Minatojima-minamimachi, Chuo-ku, Kobe, Hyogo, Japan. [3]Graduate School of Organic Material Engineering, Yamagata University, 4-3-16 Jonan, Yonezawa, Yamagata, Japan. [4]Project Research Center for Fundamental Sciences, Graduate School of Science, Osaka University, 1-1 Machikaneyama, Toyonaka, Osaka, Japan. [5]Japan Synchrotron Radiation Research Institute, Kouto, Mikazuki-cho, Sayo-gun, Hyogo, Japan. [6]Innovative Catalysis Science Division, Institute for Open and Transdisciplinary Research Initiatives (ICS-OTRI), Osaka University, Suita, Osaka, Japan. [7]The Institute of Scientific and Industrial Research, Osaka University, Ibaraki, Osaka, Japan. [8]Institute for Advanced Co-Creation Studies, Osaka University, Toyonaka, Osaka, Japan

Author contributions
Y.T. conceived and directed the study. Y.K. and R.I. performed the syntheses and spectroscopic studies. All authors contributed to the characterizations and discussion. Y. Ikemoto discussed and explained the FT-IR spectroscopy results. Y. Ishii and H.W. performed the MD simulations and explained the results. S.M. and G.M. discussed and explained the results of the SAXS measurements. M.O., O.U. and T.I. wrote a section relating to the DMA measurements. Y.K., J.P. and Y.T. cowrote the paper. A.H. and H.Y. gave valuable suggestions. Y.T. oversaw the project and contributed to the execution of the experiments and interpretation of the results.

Competing interests
The authors declare no competing interests.

Publisher's note
Springer Nature remains neutral with regard to jurisdictional claims in published maps and institutional affiliations.

Supplementary information The online version contains supplementary material available at https://doi.org/10.1038/s41427-021-00348-2.

Received: 15 August 2021 Revised: 14 November 2021 Accepted: 18 November 2021.
Published online: 22 April 2022

References

1. Appel, E. A., del Barrio, J., Loh, X. J. & Scherman, O. A. Supramolecular polymeric hydrogels. *Chem. Soc. Rev.* **41**, 6195 (2012).
2. Yan, X., Wang, F., Zheng, B. & Huang, F. Stimuli-responsive supramolecular polymeric materials. *Chem. Soc. Rev.* **41**, 6042 (2012).
3. Khare, E., Holten-Andersen, N. & Buehler, M. J. Transition-metal coordinate bonds for bioinspired macromolecules with tunable mechanical properties. *Nat. Rev. Mater.* **6**, 421 (2021).
4. Gu, Y., Zhao, J. & Johnson, J. A. A (Macro)molecular-level understanding of polymer network topology. *Trends Chem.* **1**, 318 (2019).
5. McCune, J. A., Mommer, S., Parkins, C. C. & Scherman, O. A. Design principles for aqueous interactive materials: lessons from small molecules and stimuli-responsive systems. *Adv. Mater.* **32**, 1906890 (2020).
6. Rosales, A. M. & Anseth, K. S. The design of reversible hydrogels to capture extracellular matrix dynamics. *Nat. Rev. Mater.* **1**, 15012 (2016).
7. Vatankhah-Varnosfaderani, M. et al. Mimicking biological stress–strain behaviour with synthetic elastomers. *Nature* **549**, 497 (2017).
8. Kitao, T. et al. Selective formation of end-on orientation between polythiophene and fullerene mediated by coordination nanospaces. *J. Phys. Chem. C.* **122**, 24182 (2018).
9. Uemura, T. et al. Mixing of immiscible polymers using nanoporous coordination templates. *Nat. Commun.* **6**, 7473 (2015).
10. Myung, D. et al. Progress in the development of interpenetrating polymer network hydrogels. *Polym. Adv. Technol.* **19**, 647 (2008).
11. Gong, J. P., Katsuyama, Y., Kurokawa, T. & Osada, Y. Double-network hydrogels with extremely high mechanical strength. *Adv. Mater.* **15**, 1155 (2003).
12. Ducrot, E., Chen, Y., Bulters, M., Sijbesma, R. P. & Creton, C. Toughening elastomers with sacrificial bonds and watching them break. *Science* **344**, 186 (2014).
13. Amamoto, Y., Kamada, J., Otsuka, H., Takahara, A. & Matyjaszewski, K. Repeatable photoinduced self-healing of covalently cross-linked polymers through reshuffling of trithiocarbonate units. *Angew. Chem. - Int. Ed.* **50**, 1660 (2011).
14. Burattini, S., Greenland, B. W., Chappell, D., Colquhoun, H. M. & Hayes, W. Healable polymeric materials: a tutorial review. *Chem. Soc. Rev.* **39**, 1973 (2010).
15. Burnworth, M. et al. Optically healable supramolecular polymers. *Nature* **472**, 334 (2011).
16. Chen, X. et al. A thermally re-mendable cross-linked polymeric material. *Science* **295**, 1698 (2002).
17. Cordier, P., Tournilhac, F., Soulié-Ziakovic, C. & Leibler, L. Self-healing and thermoreversible rubber from supramolecular assembly. *Nature* **451**, 977 (2008).
18. Miwa, Y., Kurachi, J., Sugino, Y., Udagawa, T. & Kutsumizu, S. Toward strong self-healing polyisoprene elastomers with dynamic ionic crosslinks. *Soft Matter* **16**, 3384 (2020).
19. Miwa, Y., Kurachi, J., Kohbara, Y. & Kutsumizu, S. Dynamic ionic crosslinks enable high strength and ultrastretchability in a single elastomer. *Commun. Chem.* **1**, 5 (2018).
20. Suckow, M. et al. Tuning the properties and self-healing behavior of ionically modified poly(isobutylene-co-isoprene) rubber. *Macromolecules* **51**, 468 (2018).
21. Sun, T. L. et al. Physical hydrogels composed of polyampholytes demonstrate high toughness and viscoelasticity. *Nat. Mater.* **12**, 932 (2013).
22. Wang, Q. et al. High-water-content mouldable hydrogels by mixing clay and a dendritic molecular binder. *Nature* **463**, 339 (2010).
23. White, S. R. et al. Restoration of large damage volumes in polymers. *Science* **344**, 620 (2014).
24. Wirthl, D. et al. Instant tough bonding of hydrogels for soft machines and electronics. *Sci. Adv.* **3**, 1700053 (2017).
25. Choi, S., Kwon, T. Woo., Coskun, A. & Choi, J. W. Highly elastic binders integrating polyrotaxanes for silicon microparticle anodes in lithium ion batteries. *Science* **357**, 279 (2017).
26. Harada, A., Hashidzume, A., Yamaguchi, H. & Takashima, Y. Polymeric rotaxanes. *Chem. Rev.* **109**, 5974 (2009).
27. Harada, A., Li, J. & Kamachi, M. The molecular necklace: a rotaxane containing many threaded α-cyclodextrins. *Nature* **356**, 325 (1992).
28. Koyama, Y. Synthesis of topologically crosslinked polymers with rotaxane-crosslinking points. *Polym. J.* **46**, 315 (2014).
29. Sawada, J., Aoki, D., Uchida, S., Otsuka, H. & Takata, T. Synthesis of vinylic macromolecular rotaxane cross-linkers endowing network polymers with toughness. *ACS Macro Lett.* **4**, 598 (2015).
30. Gotoh, H. et al. Optically transparent, high-toughness elastomer using a polyrotaxane cross-linker as a molecular pulley. *Sci. Adv.* **4**, 7629 (2018).
31. Bin Imran, A. et al. Extremely stretchable thermosensitive hydrogels by introducing slide-ring polyrotaxane cross-linkers and ionic groups into the polymer network. *Nat. Commun.* **5**, 5124 (2014).
32. Koyanagi, K., Takashima, Y., Yamaguchi, H. & Harada, A. Movable cross-linked polymeric materials from bulk polymerization of reactive polyrotaxane cross-linker with acrylate monomers. *Macromolecules* **50**, 5695 (2017).

33. Nakahata, M., Mori, S., Takashima, Y., Yamaguchi, H. & Harada, A. Self-healing materials formed by cross-linked polyrotaxanes with reversible bonds. *Chem* **1**, 766 (2016).
34. Ikura, R. et al. Supramolecular elastomers with movable cross-linkers showing high toughness based on stress dispersion. *Macromolecules* **52**, 6953 (2019).
35. Ikura, R. et al. Preparation of hydrophilic polymeric materials with movable cross-linkers and their mechanical property. *Polymer* **196**, 122465 (2020).
36. Kashiwagi, Y. et al. Linear viscoelastic studies on a transient network formed by host–guest interaction. *J. Polym. Sci. Part B Polym. Phys.* **56**, 1109 (2018).
37. Kashiwagi, Y. et al. Dynamics of the topological network formed by movable crosslinks: effect of sliding motion on dielectric and viscoelastic relaxation behavior. *Macromolecules* **54**, 3321 (2021).
38. Turley, S. G. A dynamic mechanical study of rubber-modified polystyrenes. *J. Polym. Sci. Part C. Polym. Symp.* **1**, 101 (1963).
39. Schneider, M., Pith, T. & Lambla, M. Toughening of polystyrene by natural rubber-based composite particles: part I impact reinforcement by PMMA and PS grafted core-shell particles. *J. Mater. Sci.* **32**, 6331 (1997).
40. Nomimura, S. et al. Self-healing alkyl acrylate-based supramolecular elastomers cross-linked via host-guest interactions. *Macromolecules* **52**, 2659 (2019).